Measurement of Interfacial Width in a Poly(styrene)/ Poly(2-vinylpyridine) Homopolymer Blend by Spatially Resolved Inelastic Electron Scattering

Krisda Siangchaew and Matthew Libera*

Department of Chemical, Biochemical, and Materials Engineering, Stevens Institute of Technology, Hoboken, New Jersey 07030

Received October 19, 1998; Revised Manuscript Received March 4, 1999

ABSTRACT: This research uses spatially resolved electron energy-loss spectroscopy (EELS) in a scanning transmission electron microscope (STEM) to determine an upper bound for the interfacial width of a solution-cast poly(styrene) (PS)−poly(2-vinylpyridine) (PVP) homopolymer blend. The measurement determines the fraction of nitrogen as a function of position across an unstained interface. The broadening effect of the incident-probe intensity distribution is deconvoluted from the raw data. In addition, a lower bound to the contribution of interfacial curvature to the interfacial width is estimated and also separated from the measured data. This leads to an upper bound to the interfacial width of 3.5 nm. The result is in agreement with independent measurements by neutron scattering reported in the literature. Dose-resolved measurements are made to demonstrate that the effects of mass loss during the present measurements are insignificant. Quantitative analysis of the carbon/nitrogen ratio is made on the basis of the background-subtracted C and N K-edges in PVP finding a value of 7.05 ± 0.20, in agreement with the stoichiometric value of 7.0.

Introduction

Polymer interfaces play an important role in determining the mechanical properties of homopolymer blends. These interfaces are not perfectly sharp. Their width is controlled by a balance of entropic and enthalpic forces which define the number and nature of entanglements between the two homopolymer phases. Values of interfacial width vary from a few nanometers to several tens of nanometers depending on the thermodynamics of a particular system of interest. These widths can be controlled to a considerable extent by the use of compatibilizers.

On the basis of a self-consistent mean-field approach, Helfand and Wasserman[1] developed a model describing the variation in volume fraction, ϕ, of one component as a function of position across an interface. This function has the form of a hyperbolic tangent given as

$$\Phi_A(x) = \frac{1}{2}\left\{1 - \tanh\left(\frac{2x}{a_I}\right)\right\} \quad (1)$$

The interfacial width, a_I, is related to the statistical segment length b and the Flory interaction parameter, χ, by

$$a_I = 2b/(6\chi)^{1/2} \quad (2)$$

The geometry defined by these two expressions is illustrated schematically by Figure 1. Stamm and Schubert[2] discuss the merits of this and alternate models of interfacial width in a recent review article.

A number of experimental techniques have been used to measure interfacial widths in a variety of both neat and compatibilized homopolymer systems.[2,3] Among these are neutron reflectivity and small-angle neutron and X-ray scattering,[3−5] forward recoil spectrometry (FRES),[6] secondary ion mass spectroscopy (SIMS) (e.g., ref 7), and X-ray photoelectron spectroscopy (XPS),[8] among others. These vary widely both in their requirements on specimen topology, varying from perfectly planar interfaces to arbitrary ones, and in their resolution which ranges from subnanometer in one dimension to tens of nanometers depending on the particular technique.

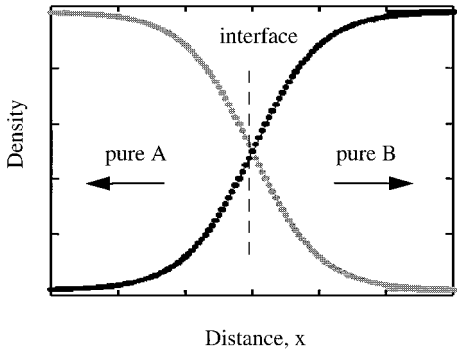

Figure 1. Hyperbolic tangent function describing the change in volume fraction of one component, $\Phi(x)$, across a polymer−polymer interface.

Neutron reflectivity has been particularly useful for the study of relatively sharp interfaces. It requires partially deuterated specimens with a planar interface which is flat over a length scale comparable to the spatial coherence length of the neutrons (∼1−10 μm). It can provide subnanometer precision in determining deuterium concentration along the direction perpendicular to the interface. Neutron reflectivity has been used to establish the interfacial width characteristic of homopolymer poly(styrene)−poly(methyl methacrylate) (PMMA) with two independent measurements giving values of order 2.0 nm.[9,10]

Discrepancies between experimentally measured values of interfacial width and those predicted by the

* Corresponding author.

10.1021/ma9816261 CCC: $18.00
Published on Web 04/13/1999

hyperbolic tangent (eq 1) or other models have been attributed to the broadening effect of capillary waves. The original model based on liquid/vapor interfaces has been extended to polymeric systems.[11−13] The average deviation of an interface from its average position can be modeled by the expression

$$\langle(\Delta z)^2\rangle = (k_B T)/(2\pi\sigma) \ln[\lambda_{max}/\lambda_{min}] \quad (3)$$

where σ is the interfacial free energy between the two polymers on either side of the interface. λ_{max} and λ_{min} define characteristic length scales associated with the geometry of the interface. λ_{max} is given in a limiting case by the lateral dimensions of the specimen which define the spectrum of possible waves present at some average temperature. In practice, however, it is determined by the length scale over which the measurement technique samples the interface. In the case of neutron scattering λ_{max} is usually taken as the neutron coherence length. λ_{min} is usually taken as the interfacial width itself. Length scales smaller than this such as a segment length in a polymer chain lead to problems in distinguishing interfacial fluctuations based on capillarity from those based on interdiffusion. Using such a formulation, there is good agreement between experimental PS/PMMA interfacial widths and those predicted by mean-field theory when the effects of capillary waves are taken into account.

Electron-scattering methods are attractive for the study of nonplanar interfaces. They can generate scattering information in both real and reciprocal space with good resolution in two dimensions rather than in just one. The interfacial width of a microphase-separated poly(styrene)/poly(diene) block copolymer, for example, has been studied on the basis of elastic electron scattering from OsO_4-stained specimens in a transmission electron microscope (TEM), in agreement with X-ray scattering studies.[14] Stains do not necessarily label a morphology in a perfectly linear fashion, however, and they will often cluster leading to inhomogenieties at length scales on the same order as interfacial widths. Hence, particularly for high-spatial-resolution electron-scattering studies, one would prefer to avoid stains and instead rely on the intrinsic interaction between the incident electron beam and the specimen itself.

This research uses spatially resolved inelastic electron scattering[15−17] based on electron energy-loss spectroscopy (EELS) to measure the interfacial width between unstained homopolymers of poly(styrene) and poly(2-vinylpyridene) (PVP). The collected signal is based on the intrinsic inelastic interaction between the incident electrons and characteristic core excitations in atomic carbon and nitrogen. After deconvoluting the effects of (1) the intensity distribution of the incident focused electron probe and (2) interfacial curvature, an upper bound for a PS−PVP interfacial width is estimated to be 3.5 nm, in agreement with recent measurements based on neutron reflectivity.[18,19]

Experimental Procedure

Solvent-cast homopolymer blends of PS−PVP were made using PS (MW = 190 000) and PVP (MW = 200 000) purchased from Scientific Polymer Products. These were dissolved at room temperature in a 7PS:3PVP weight ratio to make a 10 wt % solution in tetrahydrofuran (THF). The fully dissolved and mixed solution was poured into pure methanol. The resulting solid precipitate was removed, dried, and then annealed at 130 °C for 2 days under a vacuum of 2×10^{-6} Torr.

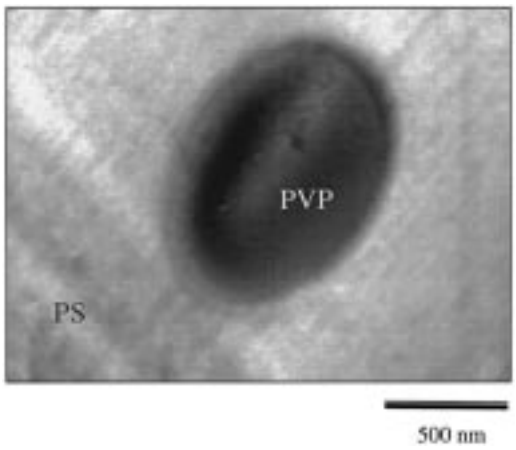

Figure 2. Bright-field TEM image of an iodine-stained PS/PVP blend. The PVP is preferentially stained and has dark contrast.

Electron-transparent specimens were cut by ultramicrotomy at room temperature using a Riechart Ultracut E microtome. The specimen thickness was measured by taking a ratio of counts in the low-loss region following the method described by Egerton.[20] Specimen thicknesses were found to be on the order of 50 nm or less. Multiple inelastic scattering effects were relatively small at these specimen thicknesses and ignored during subsequent analysis. Cut sections were collected on bare Cu grids. A subset of specimens was stained by exposing them to iodine vapor for 2 h at room temperature. Iodine preferentially labels the PVP phase, giving it dark contrast in a traditional bright-field image.[21] All work involving EELS compositional profiling was done using unstained specimens. There was sufficient contrast in annular-dark-field (ADF) STEM images based on the slight differences in PVP and PS density to identify regions of interest in unstained specimens for subsequent spectroscopic study.

Imaging and scattering experiments were performed at Stevens using a 200 keV Philips CM20 field-emission gun (FEG) scanning transmission electron microscope (TEM/STEM). This instrument is equipped with a Schottky field-emission source whose high brightness enables the formation of finely focused electron probes (∼1−5 nm full-width at half-maximum, fwhm) with sufficient current (∼0.1−3 nA) to do meaningful scattering experiments at high spatial resolution. The electron probe size for the present experiments was determined by rastering the focused beam across an oriented MgO cube[22] and recording the electron intensity elastically scattered to high angles (∼35−100 mrad). The measurement was confirmed by photographing the unscattered probe during a raster across a Gatan model 694 multiscan CCD camera. At the end of the microscope column is a Gatan model 666 parallel electron energy-loss spectrometer. This is a magnetic-prism spectrometer which uses a linear 1024 photodiode array in the electron detector.

Core-loss electron energy-loss spectra were recorded with a dispersion of 0.2 eV/channel over ranges of energy loss convenient to simultaneously record the C K-edge (284 eV) and the N K-edge (401 eV). To offset effects due to small energy drift in the electron beam, the energy scales of these core-loss spectra were all calibrated after acquisition by aligning the $1s-\pi^*$ preedge feature in the C K-edge to 284 eV. Standard background modeling based on the AE^{-r} function where E is the energy loss and A and r are constants was used. The subtraction of raw data by the background model was performed following Egerton.[20]

Results

The morphology of the solution-cast blend consists of a dispersion of PVP particles in a matrix of PS and is illustrated by the low-magnification bright-field image of a stained specimen in Figure 2. The PVP particles

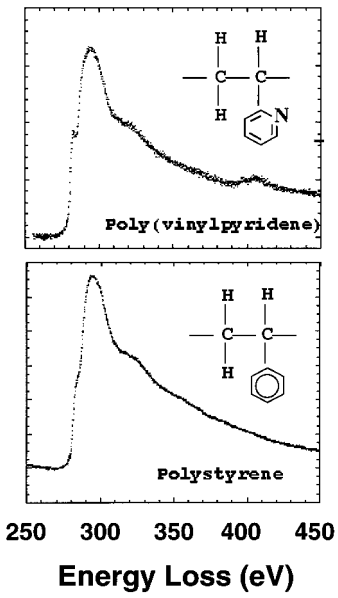

Figure 3. Core-loss electron energy-loss spectra collected from PVP and PS. The large peak ca. 290 eV loss corresponds to the carbon K-shell ionization. The spectroscopic feature at 401 eV loss corresponds to the nitrogen K-shell ionization and is evident only in the spectrum collected from PVP.

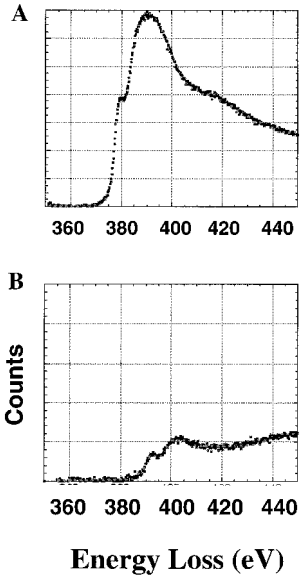

Figure 4. Background-subtracted core-loss edge of (A) carbon and (B) nitrogen collected from PVP.

are roughly spherical with diameters ranging from submicrons to a few microns. This morphology coarsened very little in response to vacuum annealing, presumably due to the high molecular weights and low mobilities of the homopolymer constituents.

In unstained specimens, one can distinguish between PS and PVP on the basis of the presence of nitrogen in the PVP (Figure 3). Nitrogen is manifested as an edge in the core-loss spectrum ca. 401 eV energy loss which is systematically absent from the PS spectrum. Figure 3 shows core-loss spectra from PVP and PS. The preedge background signal was modeled in such raw spectra, extrapolated, and removed to produce background-subtracted C−K and N−K edges. Typical examples of background-subtracted C and N core-loss spectra collected from the PVP phase are illustrated in Figure 4.

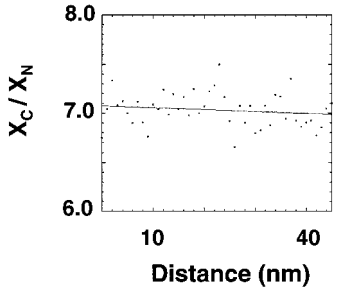

Figure 5. Carbon/nitrogen ratio (X_C/X_N) determined at different locations along a line scan in the PVP phase.

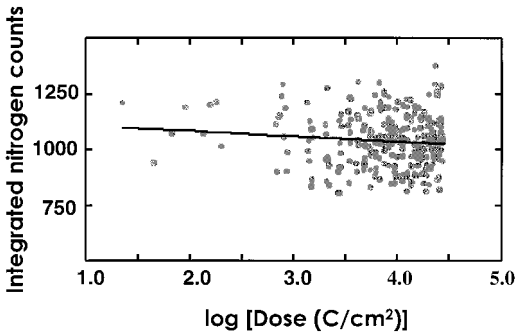

Figure 6. Integrated counts under the PVP N K-edge edge as a function of accumulated electron dose.

Background-subtracted spectra can be used to quantitatively determine the carbon-to-nitrogen ratio characteristic of PVP. This ratio (X_C/X_N) should equal 7. It can be determined using the following expression:[23]

$$\frac{X_C}{X_N} = \frac{S_C(\beta,\Delta)\,\sigma_N(\beta,\Delta)}{S_N(\beta,\Delta)\,\sigma_C(\beta,\Delta)} \tag{4}$$

where $S_C(\beta,\Delta)$ and $S_N(\beta,\Delta)$ are the experimentally measured counts from the carbon and nitrogen edges, respectively, integrated over the energy window Δ; $\sigma_C(\beta,\Delta)$ and $\sigma_N(\beta,\Delta)$ are the partial inelastic scattering cross sections; and β is the spectrometer collection angle (10 mrad). The partial inelastic scattering cross sections were calculated using a hydrogenic approximation.[20] This is a relatively robust model for which there is generally good agreement with light-element K-edges. Errors associated with the scattering cross-section calculation are expected to be similar for C and N and, hence, be minimized when taking their ratio. For an energy window of $\Delta = 30$ eV, this model calculates that $\sigma_N(\beta,\Delta) = 1.085 \times 10^{-21}$ cm^2 and $\sigma_C(\beta,\Delta) = 2.439 \times 10^{-21}$ cm^2. The ratio of X_C/X_N measured entirely within the PVP phase as a function of spatial position is shown in Figure 5. The 44 measurements in Figure 5 give an average experimental X_C/X_N value of 7.05 ± 0.20. This is in good agreement with the expected value of $X_C/X_N = 7.0$.

There was no appreciable nitrogen mass loss detected over a wide range of incident radiation dose. Mass-loss effects in various polymer systems have been studied by Egerton[24] and Briber and Khoury,[25] among others (e.g., ref 26 and references therein). Mass loss is generally attributed to radiolysis effects where ionized species find themselves in unfavorable energetic potentials and are ejected from the specimen. Figure 6 shows the integrated counts under the N edge as a function of

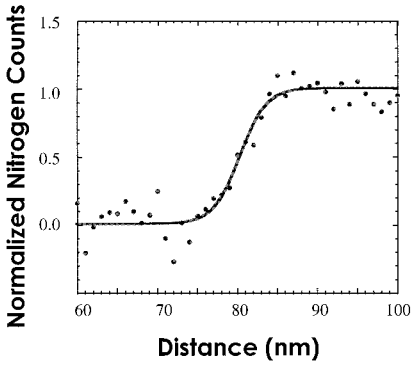

Figure 7. Normalized nitrogen counts across a PS/PVP interface. The raw data are fit to a hyperbolic tangent function (solid curve).

accumulated electron dose. The average number of nitrogen counts appears to decrease very slightly over doses ranging over more than 3 orders of magnitude. The decrease, however, is less than the average scatter in the data. If significant, it is small at its worst. The doses used to collect nitrogen profiles across PS/PVP interfaces in the present research were of order 10^3 C/cm^2. On the basis of the data of Figure 6, nitrogen loss under such a condition is insignificant.

Compositional variations across PS/PVP interfaces were measured by following the integrated N signal. One result is shown in Figure 7. The data are normalized to the average nitrogen signal measured in the bulk PVP well away from the interface, so the maximum value is unity while the minimum value is zero. A number of data sets displaying broader transitions in the nitrogen profile were also collected. As discussed below, their increased breadth is attributed to geometric effects due to random sectioning of spherical PVP particles. The data presented in Figure 7 correspond to the narrowest data set collected where, presumably, geometrical effects of interfacial curvature are minimized.

Measuring the size and shape of a focused electron probe to determine its intensity distribution $I_p(x)$ has been done by a number of methods.[27] Most involve scanning the electron probe across a sharp edge. In the present research the probe size was measured by scanning the probe across an oriented MgO cube as illustrated by Figure 8. The convergent beam electron diffraction pattern in the inset to Figure 8A shows that the cube of interest is well oriented along a [100] zone axis. The (010) plane thus lies parallel to the incident electron beam direction. The scan across the edge of this cube is indicated by the horizontal line. Figure 8B shows the electron intensity elastically scattered to high angles and collected by a solid-state detector.[28] These data indicate that the incident electron probe has a Gaussian intensity distribution (Figure 8C) with a full width at half-maximum (fwhm) of 3.5 nm. This value was independently confirmed by recording the probe image directly onto a slow-scan CCD camera and digitally measuring the intensity distribution in the image.

Discussion

The raw experimentally measured distribution of nitrogen, $R_N(x)$, does not precisely reflect the intrinsic distribution $\phi_N(x)$. $R_N(x)$ is given as a convolution of $\phi_N(x)$ with the intensity distribution of the incident electron probe $I_p(x)$ and an interfacial curvature function $C(x)$:

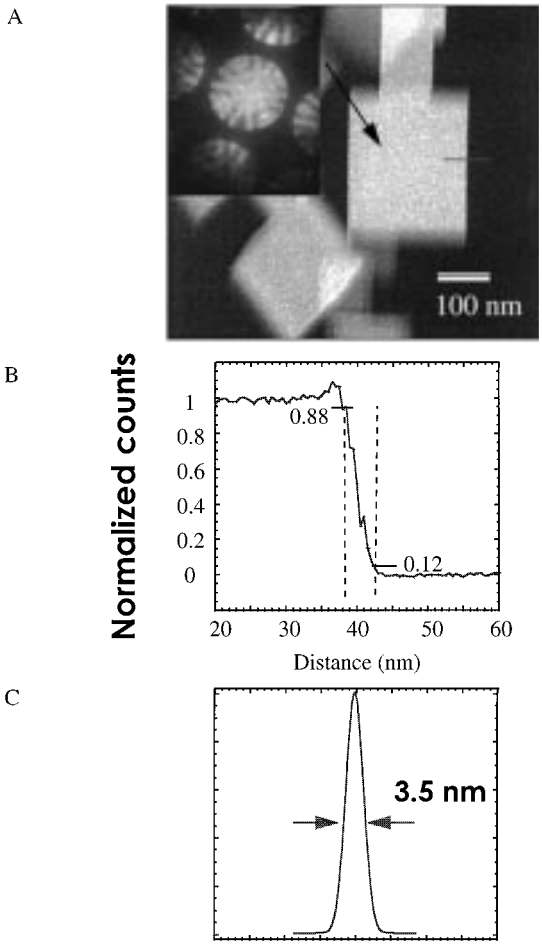

Figure 8. (A) Annular dark-field image of MgO smoke crystals with one crystal aligned with its cube face parallel to the electron beam. The inset shows a convergent-beam diffraction pattern confirming that this crystal is oriented along a [100] zone axis. (B) Variation in electron intensity scattered to high angles during a scan across the crystal edge (solid line in (A)). (C) Intensity profile of the incident focused electron probe derived from (B).

$$R_N(x) = \phi_N(x)^* I_p(x)^* C(x) \qquad (5)$$

In addition, one would expect a further contribution to the measured interfacial width due to capillary waves. These issues are discussed below.

The probe intensity distribution can be readily deconvoluted from the raw signal. $I_p(x)$ can be modeled by a Gaussian function normalized to unity with a fwhm of 3.5 nm (Figure 8). To represent the experimental data in a continuous functional form without noise, the raw data in Figure 7 were fit to a hyperbolic tangent expression. The contribution of $I_p(x)$ to the apparent interfacial width can then be removed through a Fourier-based procedure given as

$$\phi_N(x) = F^{-1}[F\{R_N(x)\}/F\{I_p(x)\}] \qquad (6)$$

where F represents a Fourier transform. The result is presented in Figure 9. Defining the interfacial width in the same fashion as done in the mean-field approach (see Figure 1), the width of this interface is 4.5 nm.

A further correction to the measurement of interfacial width concerns the effect of interfacial curvature. Not

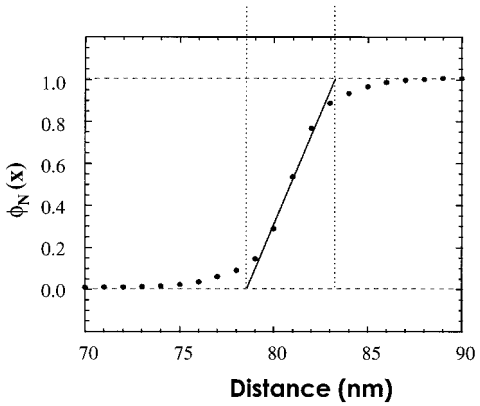

Figure 9. PS/PVP interfacial profile after the effect of finite probe size was deconvoluted.

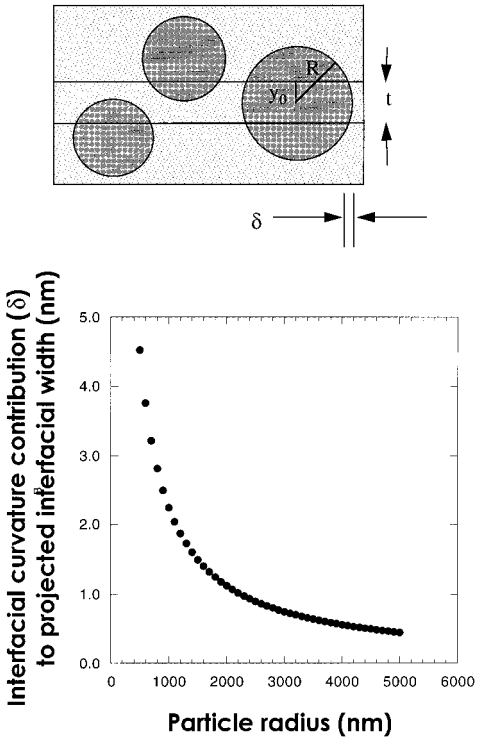

Figure 10. (A, top) Schematic illustrating a TEM section of thickness t cutting across several particles, one of which has a radius R. (B, bottom) Simulation of the effect of particle radius on the projected interfacial width for a fixed section thickness of 50 nm.

included in the deconvolution procedure of eq 6 is the contribution of the projected interfacial curvature represented by $C(x)$. Varying $C(x)$ influences the projected interfacial width as seen when the probe is rastered across the particle/matrix interface. As illustrated by Figure 10A, a thin electron-transparent section is cut from a bulk piece of material with a dispersion of roughly spherical PVP particles in a continuous PS matrix. The projected interfacial curvature contribution, $C(x)$, to the measured profile $R_N(x)$ will depend on the position of the section in the dispersed particle, the size of the particle, and the section thickness.

The projected curvature function $C(x)$ can be calculated for various possible combinations of particle size, section thickness, and section position. The geometry for such a calculation is illustrated by Figure 10A. A sphere of radius R is cut by a section of thickness t. The position of the cut relative to the position of the sphere is given by the value of y_0. The function $C(x)$ is given by the fraction of projected density of the spherical phase over the thickness of the section as a function of position. The result of one particular calculation is presented in Figure 10B for the case of $y = t/2$ where a section of thickness of 50 nm samples the middle of a dispersed particle. For the purposes of this calculation, the contribution, δ, to the projected interfacial width is defined as the length over which $C(x)$ rises from 0.05 to 0.95. Figure 10B shows that δ increases substantially as the particle size R decreases. δ becomes increasingly significant for thicker sections which sample top or bottom portions of a dispersed particle ($y_0 \sim R$). In the opposite extreme where R is relatively large, t is small, and y_0 is close to $t/2$ (i.e., the section samples the middle of the sphere) δ would be relatively small.

The fact that a range of interfacial widths was measured during this research supports the fact that the interfacial curvature can affect the measurement. The data presented in Figure 9 correspond to the data set with the sharpest transition. This set presumably most closely samples the center portion of a large dispersed PVP particle. The other profiles, with transitions ranging up to 10 nm or more in some cases, presumably correspond to sections that sample PVP particles near their top or bottom or from relatively small particles (diameters ca. 0.5 μm and below). The diameter of the PVP phase used to produce Figure 9 was approximately 2.0 μm. On the basis of the intensity of inelastic electron scattering in the low-loss region, the corresponding section thickness was estimated to be 30−40 nm. Assuming the section sample a PVP particle near its center, a lower bound to the curvature contribution δ to the interfacial width for the data in Figure 9 would thus be 1 nm (Figure 10B). Hence, an upper bound to the experimentally determined width of the PS−PVP homopolymer interface as measured by spatially resolved energy-loss spectroscopy is thus $a_I^{PS-PVP} = 3.5$ nm.

When comparing the value of 3.5 nm determined by the present research to values in the literature, one must further take into account the effects of polymer architecture and molecular weight as well as sample preparation. Dai, Norton, and Kramer[18] measured a value of approximately 3.4 nm by neutron scattering from PS−PVP homopolymer bilayer specimens. They studied interfaces between homopolymers of deuterated PS (MW = 105K, degree of polymerization (dp) = 1010) and PVP (dp ~ 2000). The present research studied PS and PVP homopolymer with dp values of 1825 and 1905, respectively. An entangled interface will narrow with increasing polymer molecular weight (e.g., 29), and one could thus argue that an additional, presumably small, correction should be made to account for the difference in MW of the PS homopolymer between these two experiments. Torikai et al.[19] studied dPS−PVP diblock copolymer with PS and PVP molecular weights of 95 000 and 72 000, respectively. Here again the effects of molecular weight and perhaps the additional effects of chain ends and midblock localization must be taken into account. Torikai et al.[19] report an interfacial width of 4.5 nm in this system (Karim, A., personal communication). In all cases, the molecular weights of the PS and PVP components are well beyond their respective homopolymer entanglement molecular weights. In all three experiments, specimens were vacuum annealed for extended periods at temperatures above T_g for both the

PS and PVP. Residual solvent is unlikely to be affecting the measurements. Presumably the anneals are sufficient for the interfaces to approach their limiting degree of entanglement.

An interfacial width due solely to thermodynamic effects, ${}^{F-H}a_I$, can be estimated using the Helfand−Wasserman approach (eq 2). Using a statistical segment length of 0.67 nm and a Flory−Huggins interaction parameter of $\chi = 0.11$ given by Shull et al.,[11] one can estimate a value of ${}^{F-H}a_I^{PS-PVP} = 1.7$ nm. Torokai et al.,[19] using slightly different values of b and χ, estimate ${}^{F-H}a_I^{PS-PVP} = 2.4$ nm. The discrepancy between experimentally measured and thermodynamically predicted interfacial widths in the case of PS−PMMA has been attributed to the broadening effects of capillary waves at the interface.[11,13] Capillary waves may be responsible for the observed differences in the experimentally measured and thermodynamically predicted interfacial widths characteristic of the PS−PVP system as well. A future electron-scattering experiment may be able to provide useful insight into the magnitude of the contribution of capillary waves to the measured interfacial width. One could expect that λ_{max} in eq 3 would scale with the specimen thickness (∼50 nm) in an electron-scattering experiment and, hence, be less than the value given by the neutron coherence length (∼1−10 μm). On the basis of eq 3, the capillary contribution to the measured interfacial width would be approximately a factor of 2 smaller in the electron-scattering experiment. Hence, an experiment using both electrons and neutrons to study planar specimens, where the complicating effects of interfacial curvature can be avoided, may be able to distinguish the capillary contribution from the thermodynamic contribution to interfacial width.

While the influence of interfacial curvature complicates the detailed study of this narrow homopolymer interface, there remain important circumstances where curvature effects would be less significant. For example, in the case of a compatibilized interface, a sized polymer/adherend interface, or a two-phase polymer system close to a disordering temperature, interfaces can become substantially diffuse. A trend to increasing interfacial width was clearly observed, for example, by Dai et al.[18] when PS−PVP diblock was added to homopolymer PS/PVP bilayers. Under such conditions, the roughly few-nanometer broadening contribution due to curvature may well be negligible while the ability to collect spatially resolved chemical data from a nonplanar system might easily justify the use of a focused-probe approach.

Conclusions

Position-resolved EELS was used to measure the PS/PVP interfacial width in a solution-cast PS−PVP homopolymer blend with the following observations:

1. PS and PVP can be quantitatively distinguished by the presence/absence of a nitrogen K-edge in an electron energy-loss spectrum without heavy element stains.

2. A 3.5 nm interfacial width was measured across the solvent-cast blend of PS/PVP. This is greater than predicted by Helfand−Wasserman theory but agrees well with recent neutron studies on PS/PVP lamellar block copolymer interfaces.

3. Spatially resolved inelastic electron scattering may enable experiments that separate capillary effects from the interfacial width defined by system thermodynamics.

Acknowledgment. The authors thank P. Prayoonthong and S. Wang at Stevens for preparing the samples. This work is supported by the Army Research Office (grants DAAH04-93-G-0239 and DAAG55-97-1-0137) and uses instrumentation jointly funded by the National Science Foundation and the New Jersey Commission on Science and Technology.

References and Notes

(1) Helfand, E.; Wasserman, Z. R. In *Developments in Block Copolymers-1*; Goodman, I., Ed.; Applied Science: London, 1982; p 99.
(2) Stamm, M.; Schubert, D. In *Annual Review of Materials Science*; Wessels, B. W., Kaufmann, E. N., Giordmaine, J. A., Wachtman, J. B., Jr., Eds.; Annual Reviews Inc.: Palo Alto, CA, 1995; p 325.
(3) Russell, T. P. *Annu. Rev. Mater. Sci.* **1991**, *21*, 249−268.
(4) Hashimoto, T.; Todo, H.; Itoi, H.; Kawai, H. *Macromolecules* **1977**, *10*, 377−384.
(5) Higgins, J. S.; Benoit, H. C. *Polymers and Neutron Scattering*; Clarendon Press: Oxford, 1994.
(6) Kramer, E. *MRS Bull.* **1996**, *21* (1), 37−42 and references therein.
(7) Wool, R. P. *Polymer Interfaces: Structure and Strength*; Hanser/Gardner: Munich, 1995.
(8) Zhuang, H.; Gardella, J. *MRS Bull.* **1996**, *21* (1), 43−48 and references therein.
(9) Fernandez, M. L.; Higgins, J. S.; Penfold, J.; Ward, R. C.; Shackleton, C.; Walsh, D. J. *Polymer* **1988**, *29*, 1923−1928.
(10) Anastasiadis, S. H.; Russell, T. P.; Satija, S. K.; Majkrzak, C. F. *J. Chem. Phys.* **1990**, *92* (9), 5677−5691.
(11) Shull, K.; Mayes, A.; Russell, T. *Macromolecules* **1993**, *26*, 3929−3936.
(12) Kerl, T.; Klein, J.; Binder, K. *Phys. Rev. Lett.* **1996**, *77*, 1318−1320.
(13) Sferrazza, M.; Xiao, C.; Jones, R.; Bucknall, D.; Webster, J.; Penfold, J. *Phys. Rev. Lett.* **1997**, *78* (19), 3693−3696.
(14) Spontak, R. J.; Williams, M.; Agard, D. *Macromolecules* **1988**, *21*, 1377−1387.
(15) Hunt, J. A.; Williams, D. B. *Ultramicroscopy* **1991**, *38*, 47−73.
(16) Jeanguillaume, C.; Colliex, C. *Ultramicroscopy* **1988**, *28*, 252.
(17) Siangchaew, K.; Libera, M. *Microsc. Microanal.* **1997**, *3*, 530−539.
(18) Dai, K. H.; Norton, L. J.; Kramer, E. J. *Macromolecules* **1994**, *27*, 1949−1956.
(19) Torikai, N.; Noda, I.; Karim, A.; Satija, S. K.; Han, C. C.; Matsushita, Y.; Kawakatsu, T. *Macromolecules* **1997**, *30* (10), 2907−2914.
(20) Egerton, R. F. *Electron Energy Loss Spectroscopy in the Electron Microscope*, 2nd ed.; Plenum: New York, 1996.
(21) Washiyama, J.; Kramer, E. J.; Hui, C. Y. *Macromolecules* **1993**, *26*, 2928−2934.
(22) Cowley, J.; Huang, Y. *Ultramicroscopy* **1992**, *40*, 171−180.
(23) Leapman, R. In *Transmission Electron Energy Loss Spectrometry in Materials Science*; Disko, M. M., Ahn, C. C., Fultz, B., Eds.; TMS: Warrendale, PA, 1992; pp 47−83.
(24) Egerton, R. F. *J. Microsc.* **1982**, *126* (1), 95−100.
(25) Briber, R.; Khoury, F. *J. Polym. Sci., Part B: Polym. Phys.* **1988**, *26*, 621−636.
(26) Reimer, L. *Transmission Electron Microscopy*, 3rd ed.; Springer-Verlag: Berlin, 1993.
(27) Weiss, J. K.; Carpenter, R. W.; Higgs, A. A. *Ultramicroscopy* **1991**, *36*, 319−329.
(28) Libera, M.; Ott, J.; Siangchaew, K. *Ultramicroscopy* **1996**, *63*, 81−91.
(29) de Gennes, P.-G. In *Physics of Polymer Interfaces;* Sanchez, I. C., Ed.; Butterworth-Heinemann: Boston, 1992; pp 55−71.

MA9816261